Not to appear in Nonlearned J., 45.

How many active galaxies and QSOs will future Space Missions detect?

Paola Andreani

INAF - Osservatorio Astronomico di Padova, vicolo dell'Osservatorio 5, I-35122 Padova, Italy

andreani@pd.astro.it

Luigi Spinoglio

Istituto di Fisica dello Spazio Interplanetario, CNR via Fosso del Cavaliere 100, I-00133 - Roma, Italy

luigi@ifsi.rm.cnr.it

and

Matthew A. Malkan

Physics and Astronomy Department, University of California, Los Angeles, CA, USA

malkan@astro.ucla.edu

ABSTRACT

Averaged spectral energy distributions (SEDs) of *active and starburst galaxies* from the 12 μm sample in the Local Universe and *quasars*, from an optically selected sample at a mean redshift $\langle z \rangle$=0.7 are built from optical, near-IR and far-IR (IRAS and ISO) photometric observations. These SEDs are then used to predict at various redshifts the number of Seyfert type 1 and type 2, starburst, normal galaxies, and quasars, that will be detected by future Space Missions dedicated to far-infrared and submillimeter astronomy, like SIRTF and Herschel. These predictions are then compared with the expected capabilities and detection limits of future deep far-IR surveys. Possible ways to identify AGN candidates on far-IR colour-colour plots for follow-up observations are then explored.

Subject headings: AGN - active galaxies: ISM, photometry - ISM: dust, extinction, - Quasars: general - continuum - infrared: galaxies, galaxies: active – photometry – Seyfert – starburst

1. Introduction

Surveys in the far-infrared (FIR) and sub-millimetre (submm) region from future space missions will provide crucial information on star formation and galaxy formation and evolution. If AGN were in place roughly at the same time as galaxies, it is natural to expect that these surveys will shed light on the AGN role in the early evolution of galaxies (Silk & Rees 1998; Granato et al. 2001).
Both AGN and star formation are characterized by a strong FIR emission both in the continuum and in molecular and atomic lines, because of the dusty and gaseous environment where they release their energy. An early dust-enshrouded phase of AGN is expected, but is missed in current surveys based on other techniques. The optical AGN phase could occur late in the process of QSO formation, corresponding to the exhaustion of the gaseous-dusty shroud inside which the host galaxy formed.

The original 12μm active galaxy sample (Spinoglio & Malkan 1989; Rush et al 1993) provided a complete and largely unbiased sample of local active galaxies. It is relatively free from the strong selection effects of optical-UV surveys, which are biased in favor of type 1 AGN, and far-IR surveys, which are biased in favor of dusty type 2 AGN and starburst galaxies. It is one of the largest homogeneously-selected samples of Seyfert galaxies available, and appears to contain representative populations of galaxies with type 1 and type 2 optical spectra (see also Tran 2001, Thean et al., 2001). The selection was done at 12μm because this band contains a constant fraction of bolometric flux for active galaxies ($\sim 1/7$). The 12μm selection is therefore the best approximation so far available to a selection at a bolometric flux limit, for the different types of active galaxies. The resulting active galaxy sample contains 53 Seyfert type 1 galaxies (hereafter Seyfert 1's), 63 Seyfert type 2 galaxies (hereafter Seyfert 2's), two blazars and 38 high-luminosity non-Seyfert galaxies out of a sample of 893 galaxies (RMS).

Little is known about the FIR properties of type 1 higher redshift objects. Because of their faintness in this energy domain they lack homogeneous samples and information is still scant (Hooper et al. 1999; 4; Polletta et al. 2000). Type 2 AGN are much more difficult to find, and are missed in classical searches.
In this work we make use of a homogenous data sample of optically selected type 1 AGN (Andreani et al. 2003) which was observed at far-IR wavelengths. We make predictions of number counts and luminosities that future FIR and submm space missions– SIRTF (Space InfraRed Telescope Facility, NASA) and the Herschel Space Observatory (Herschel, ESA)– will be able to detect.

For local galaxies we adopted the spectral energy distributions (SEDs) of homogenous subsamples extracted from the 12μm galaxy sample: Seyfert 1's, Seyfert 2's, starburst

and normal galaxies for which Infrared Space Observatory (ISO) photometry was collected (Spinoglio et al. 2002). For higher redshift type 1 AGN, we chose the optically selected sample at a mean redshift of $< z >$=0.7 observed in the FIR by Andreani et al. (2003).

2. Expected counts of Type 1 AGN and Active Galaxies

As it is well known, number counts of extragalactic objects are a fundamental tool for investigating evolution, since they are related to the Luminosity Function of the population, as a function of redshift. The differential number counts, $dN(S)/dS$, (sources/unit flux interval/unit solid angle) can be expressed as an integral of the epoch-dependent luminosity function, $\Psi(L, z)$:

$$\frac{dN}{dS} = \int_{z_l}^{z_u} dz \frac{dV}{dz} \frac{dL(S,z)}{dS} \Psi[L(S,z), z] \qquad sources/sr \tag{1}$$

where z_u and z_l are the effective upper and lower limits of the redshift distribution, and $\frac{dV}{dz}$ is the differential comoving volume. The integrated counts are found by integrating eq.1 to different flux limits, S.

To predict the differential and integral number counts of active galaxies and quasars we need to compute equation 1 with the following assumptions:

- The geometry of the Universe: we use two different models both with H_0=75 km/s/Mpc: (1) $\Omega = 1$, $\Omega_\Lambda = 0$ and (2) $\Omega = 1$, $\Omega_\Lambda = 0.7$ and $\Omega_{mat} = 0.3$. They have been chosen because their predictions represent two extreme cases.
- The SEDs of the populations: we take the empirical optical-far-IR SEDs of active galaxies and QSOs (see § 2.1) and assume that they are luminosity-independent. The only difference between normal and starburst galaxies is the luminosity break. This simplified assumption avoids more complicated situations where the SED continuously changes with luminosity.
- The Local Luminosity Function (LLF): we consider different LLFs as empirically determined for the different classes: AGN, starburst and normal galaxies (see § 2.2).
- The form of the LF evolution: different evolution laws are used for each class (see § 2.3).

In the following sections we discuss each of these assumptions.

2.1. Far-IR SEDs of Quasars and Seyfert galaxies

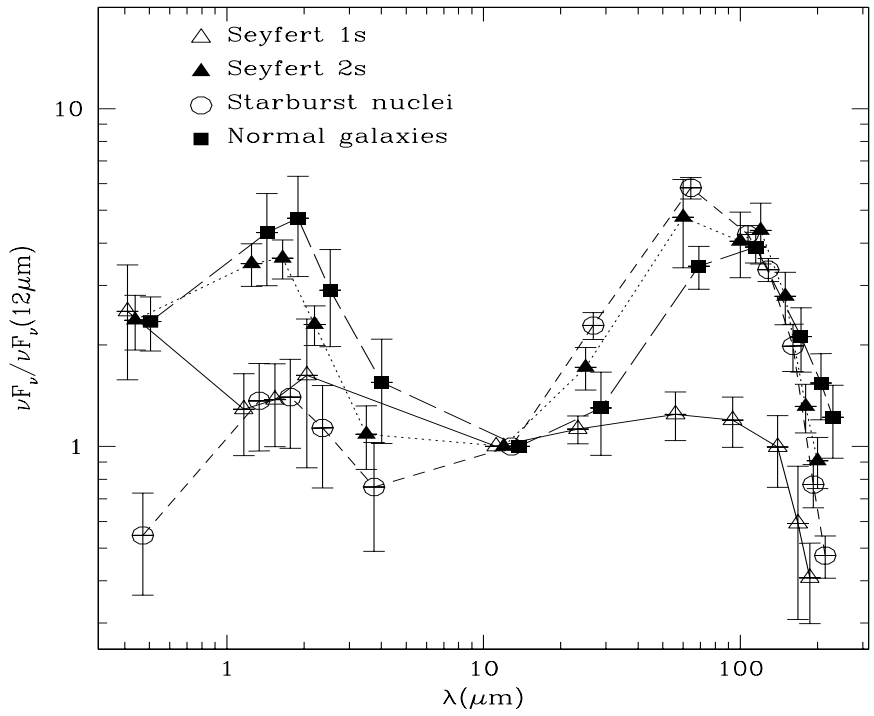

Fig. 1.— Average SEDs of Seyfert, Starburst and Normal Galaxies normalized to 12μm. From Spinoglio, Andreani, Malkan (2002).

Based on the results of Spinoglio, Andreani and Malkan (2002), Figure 1 shows the observed average SED of the different classes of galaxies in the Local Universe, normalized to 12μm. Seyfert 1's have the flattest SED throughout the entire wavelength range, with the relatively weakest FIR emission. Seyfert 2's show two pronounced peaks: at 100μm and 1.6μm. Starburst galaxies show the brighter peak at 60μm and the weaker one at 1.6μm, showing that recent and ongoing star formation–detected in the FIR–outshines the old stellar populations, which peak in the H band. Normal galaxies show again the same two peaks.

For this work we need to assume an evolutionary law for AGN, but Seyfert 1's lack of a good empirical determination of their redshift evolution. Fortunately, the evolution of their higher redshift analogs–type 1 QSOs–is well determined. Their far-IR SED is however less well defined. In this work we take the composite SED derived from optical, near-IR and FIR photometry of an optically selected sample of QSOs. Figure 2 shows the average spectrum in the QSO restframe, normalized at $\lambda_{\rm blue} = 0.44\,\mu$m. It has a well defined IR component

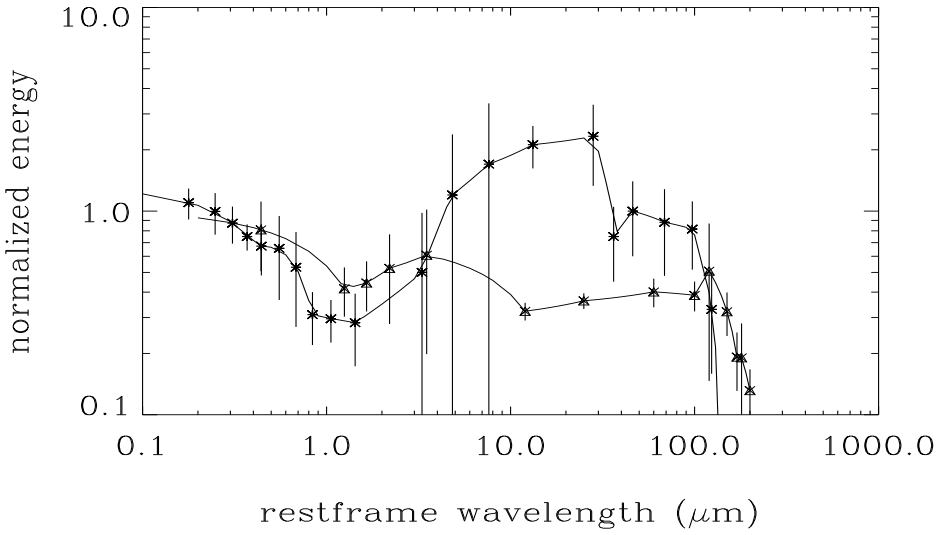

Fig. 2.— The average QSO spectrum (adopted from Andreani et al., 2003) compared with that of Seyfert 1's. Both spectra are normalized at $\lambda_{\rm blue} = 0.44\,\mu$m. Triangles correspond to Seyfert 1 data, asterisks to QSOs. Solid lines show the interpolating curves.

peaking at 10-30 μm and dropping steeply towards $100\,\mu$m. The errorbars shown are those related to the averages, but also include photometric uncertainties.

Seyfert 1's and QSOs belong to the same class of objects, type 1 AGN, with Seyfert galaxies populating the low luminosity end of the luminosity function. Figure 2 shows also a comparison of the observed Seyfert 1's SED with that of QSOs. Within the errorbars, no large differences are present, both below a few microns and above $100\,\mu$m. The QSO thermal spectrum has a steeper turnover in the FIR range, and more power between 10 and $30\,\mu$m compared to the Seyfert 1's SED. QSO SED shows higher average dust temperature (100-150 K), with respect to Seyfert 1's (22-70K) (Spinoglio et al. 2002). Because of their selection criteria, this difference could be ascribed to a luminosity effect. We lack high-z object data to disentangle this effect from an evolutionary behaviour.
Note that the QSO SED is quite different from Seyfert 2's. This latter has a large far-IR emission shifted to longer wavelengths, and a second bump in the near-IR, which is not present in QSOs (see Figure 1).

To compute the K-corrections, i.e. $dL(S,z)/dS$ in equation 1, we use for each class its appropriate composite spectrum as shown in Figures 1 and 2.

2.2. The Luminosity Functions

For the Local Luminosity Function (LLF), $\Psi_0(L)$, we adopt the 12μm LLF for Seyfert, starburst and normal galaxies (RMS). There is some uncertainty about the space densities at the low luminosity end, because no explicit correction for the over-concentration of local galaxies in Virgo was applied. Fang et al. (1998) and Xu et al. (1998) provide slightly different parameters, but all 3 of those 12 μm LLFs are in reasonable agreement around $L_\star$ galaxies, which dominate the counts. We use the same LLF shape with the different parameters given by RMS for the different classes: Seyfert 1's and 2's, and non-Seyferts (starburst and normal galaxies).

This 12 μm 'Seyfert 1' LF is in principle supposed to include quasars in it, as it was computed for a sample that includes 3C 273. As a practical limitation, though, it is too insensitive and thus covers too small a volume to define the highest end of the Sy1/QSO LF. It also does not take into account the AGN evolution which is, on the contrary, included in the QSO LF. Therefore, to extend the Sy1 LF to higher luminosities, and to include the luminosity-number density evolution of these objects we use the B-band luminosity function computed by Boyle et al. (2001) (see also La Franca and Cristiani, 1998). We assume that a constant relation exists between the B-band LF and the far-IR one. This latter has been applied to both type 1 AGN (Seyfert 1's and QSO).

The Seyfert 1's and QSO used in this work were selected in different ways, and the corresponding LF differs slightly in shape. In Figure 3 the QSO LF is shown (solid line) superposed on that of the Seyfert 1's (dotted line). Both LFs are computed at a redshift of 0.3, the minimun redshift for which a reliable QSO LF exists. The Seyfert 1 LLF was evolved from redshift 0 to a redshift of 0.3, according to the prescriptions described in §2.3.

As shown in Figure 3 the bright end of the QSO LF is slightly steeper (the slope exponent being -2.5) than Seyfert 1's (-2.2). However, within the errorbars this difference is not significant. The knee at $L_\star$ differs and that of QSOs falls at higher luminosity (log $L_\star \sim$10.5). At the faintest luminosities, the two LF slopes coincide but the amplitudes differ by a factor of 10. This high luminosity knee and the lower numbers at lower luminosities for QSOs can be explained since nearly all QSO samples are based on integrated properties of stellar-looking objects. When the host galaxy starts becoming important, the object is no longer classified as a QSO, but rather a Seyfert'1. The best approximation of the type 1 luminosity function would be to adopt (see Figure 3) the QSO LF above $\log L_\star \sim 10.5$ and then the relatively steep Seyfert 1's below that, where they cross over.

Thus, for the sake of completeness we use, when computing the expected number counts for Seyfert 1, two LFs: that of QSO and that given by RMS for Seyfert 1.

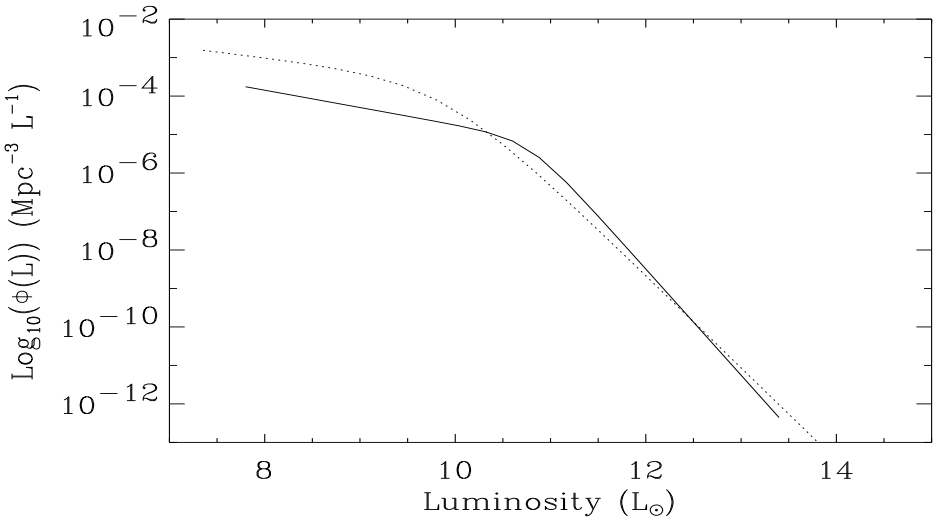

Fig. 3.— The QSO LF (solid line) computed at a redshift of 0.3 is compared with the Seyfert 1 12 μm LF (dotted line) evolved in redshift as explained in section 2.3. The x-axis is logarithm of object luminosity in solar luminosity.

2.3. The Evolution

QSOs have a strong evolution, which is known at least up to redshift 3. We adopt the redshift evolution of the LF, $\Psi(L, z)$, described by Boyle et al. (2001) up to redshift 3, and modified by Bianchi, Cristiani & Tae-Sum (2001), whose model has a down-turn at $z = 3$ and an exponential decay until $z = 10$. For starburst and Seyfert galaxies we follow the prescriptions of Malkan and Stecker (1998, 2001, hereafter MS01), who introduce a luminosity evolution into the LLF:

$$\Psi(L(\nu), \nu; 0) = C(\frac{L}{L_\star})^{1-\alpha}[1 + (\frac{L}{\beta L_\star})^{-\beta}]\frac{d\log\phi_{60}}{d\log\phi(\nu)} \quad (2)$$

where pure luminosity evolution is assumed, with luminosity scaling as $(1+z)^Q$ up to redshift z_{break}, no further evolution for $z_{break} \leq z \leq z_{max}$ and a cutoff at z_{max}=4. We adopt the parameters of their *baseline* model: Q=3.1 and z_{break}=2.

Since Seyfert 1's can be considered as either low-luminosity type 1 AGN or local type 1 active galaxies, we tried two possible evolutionary laws for this class: the first one from MS01, the same used for Seyfert 2's; the second one from Boyle et al. (2001), the same used for QSOs.

Table 1 summarizes the adopted laws.

Our definition of normal galaxies consists of all objects not showing any sign of activity, below a luminosity cut-off of $L_{IR} < 6 \times 10^{44}$ erg s^{-1} (Rush et al 1993). Most of them are then late-type galaxies, whose evolution is assumed to be milder (Franceschini 2000). For this class a different evolution law is then applied with a lower exponent, Q=2.

Recently it has been suggested that far-IR spectra of high redshift galaxies do not show evidence for any strong evolution with respect to local counterparts (Chapman et al., 2002; Lagache, Dole, Puget, 2002). Since at high redshifts we only detect the most luminous sources, it is not currently possible to disentangle this finding from luminosity effects. In other words, with the present data sets our knowledge of how a galaxy goes through subsequent stages of evolution is too scanty. Whether galaxy evolution is driven from number density or pure luminosity evolution cannot be settled.
Because of our poor knowledge of galaxy evolution, we simply let the population of normal galaxies have a milder evolution than starbursts.

We list for clarity in Table 1 the adopted laws for SEDs, LLFs and evolution for each class of objects.

3. How many galaxies will SIRTF and Herschel detect ?

Tables 2 and 3 predict the counts in the filter bands of IRAC and MIPS on board of SIRTF and PACS on board of Herschel. Wavelengths and flux limits are given by the estimated instrument sensitivity [1]. The exepcted survey sky area and counts for the different galaxy classes are shown. Table 2 refers to $\Omega_\Lambda = 0$ and $\Omega = 1$, Table 3 to $\Omega_\Lambda = 0.7$ $\Omega_{mat} = 0.3$. In both cases H_0=75 km/s/Mpc.

Counts are computed by integrating down to the instrument sensitivity over the given sky area. We computed the counts in the bands at 110 and 170 μm only for Seyfert, starburst and normal galaxies. The empirical QSO SED built on QSO photometry does not extend to these long wavelengths in the QSO restframe. Consequently the counts cannot be computed unless assumptions about the form of the long wavelength spectrum are made.

Tables 2 and 3 clearly show that the number counts strongly depend on Universe geometry. In a flat Λ-dominated Universe the surface density of galaxies is larger. Open Cosmologies increase all the counts by at least one order of magnitude in general. This effect

[1] from Väisänen (2001), SIRTF web-page: sirtf.caltech.edu and PACS web-page: pacs.ster.kuleuven.ac.be

is due to the larger available comoving volume which is only partially offset by the decrease in object number density in the luminosity function (see eq. 1). there is a larger comoving volume for a given surface area on the sky, and therefore a larger surface density of high-z objects.

Two different LFs and evolutionary laws are adopted for Seyfert 1's, and the corresponding results are listed in two columns in tables 2 and 3. Column 6 shows the predicted counts using the RMS local LF as explained in section 2.2 and evolved as in section 2.3. Column 5 shows instead the Seyfert 1 counts computed using the QSO LF and integrating with an upper integration limit corresponding to M_B=-23 (as Seyfert 1's are considered complementary to optical QSOs with respect to luminosity). We find more 'Seyfert' galaxies than 'quasars' by one order of magnitude at short wavelengths (4.5 and 8 μm) for both choices of the LFs, but their numbers coincide at 24 and 75 μm. Furthermore, quite similar numbers of Seyfert 1's are found (as listed in columns 5 and 6) although computed using two different LFs (see Figure 3).

'Starbursts' outnumber the active galaxies at all wavelengths, but the difference between the two populations shrinks as one goes from short to long wavelengths. This is as expected, since the normal galaxy SED is relatively brighter at the longest FIR wavelengths than the starburst SED.

Malkan and Stecker (MS01) obtained similar results. They predict 914 galaxies in 0.3deg^2 (9.1 $\times 10^{-5}$ sr) for the *baseline* case (Q=3.1 luminosity evolution index) at 25 μm, 5483 galaxies in 1 deg^2 (3×10^{-4} sr) at 100 μm 16,144 galaxies and at 200 μm. At these faint levels MS01's counts are dominated by SB galaxies, and are only a little lower (roughly 30%) than the predicted counts in tables 2 and 3. Also at 6 μm MS01's prediction are a little lower, but not seriously inconsistent. The general conclusion is that the agreement between the two model predictions of starburst and normal galaxies is satisfactory.

Figures 4 and 5 plot the expected differential counts for QSOs, Seyfert, starburst and normal galaxies in the SIRTF observing bands: 4.5, 8, 24, 75, 110 and 170 μm for the two Universe models considered in this work.
The QSO counts break at fluxes around 0.1-1 mJy, since the integration of equation 1 has a low luminosity cut-off at M_B=-23. This cut-off was introduced to distinguish QSOs from Seyfert galaxies, and because the QSO LF is determined down to this absolute blue magnitude. This means that in future surveys *all* type 1 QSOs up to redshift 10 (those with $M_B \leq$ -23) will be detectable.

As expected, starbursts dominate the counts at all fluxes and all wavelengths. Seyfert

counts show a flatter slope at low fluxes. Seyfert 1 counts grow more steeply than the Seyfert 2's at low fluxes at almost every wavelength.
Seyfert 1's and 2's are almost indistinguishable at 170 μm where fluxes are very likely due to the host galaxies. At λ >24 μm Starbursts and normal galaxies show steeper slopes at low fluxes. Because of our assumptions on their milder evolution, the galaxy contribution to counts is smaller at all wavelengths from a factor of 3 at low fluxes up to two orders of magnitude at large fluxes. At low fluxes and long wavelengths we expect a non-negligible contribution from normal galaxies, although starburts keep dominating the counts. Starburst counts increase more steeply than Seyferts and behave as Seyfert 2's at 4.5 and 8 μm, except at low fluxes, where Seyfert 2's have a flatter slope.

4. What luminosities will future space missions detect?

To explore the capabilities of future space missions we make the simple exercise in Figure 6 of comparing the expected sensitivities of various instruments with the SEDs observed at redshifts 0 and 10. We assume first that the observed SED does not change with lookback time, and no evolution occurs in luminosity (see panel (a)). We then take two naive evolutionary models: the first one with a luminosity evolution proportional to the second power of the redshift (L $\propto$ (z + 1)^2) (see panel (b)) and the second one proportional to the third power of the redshift (L $\propto$ (z + 1)^3) (see panel (c)). Figure 6 shows the flux distribution that a starburst galaxy of a given luminosity in the Local Universe would have at different redshifts, assuming the three different luminosity evolution laws. The predicted SEDs are then compared with the expected sensitivities of the future IR/submillimeter space missions, namely SIRTF, Planck, Herschel, ASTRO-F and NGST. The first panel (Fig.6a) shows that a starburst galaxy with a bolometric luminosity of 10^{12} L$_\odot$ can be detected (at 5 σ in 1 hr) by SPIRE and ASTRO-F at a redshift z=1; by PACS almost at a redshift z $\simeq$ 2 at the longest wavelengths; by SIRTF at redshift between 1 and 3, from long to short wavelengths, respectively; by NGST at a hypothetical redshift close to 10. Similarly, the second panel (Fig.6b) shows that a starburst with a zero-redshift bolometric luminosity of 5 $\times$ 10^{11} L$_\odot$– assuming a luminosity evolution proportional to the second power of the redshift–would be detected by SPIRE on Herschel at a redshift close to z $\simeq$ 4; by ASTRO-F at z $\simeq$ 2; by PACS at z $\simeq$ 3; by SIRTF at a redshift between 2 and 5, from long to short wavelengths, respectively; by NGST at any redshift. Finally the third panel (Fig. 6c) shows that a starburst with a zero-redshift bolometric luminosity of 10^{11} L$_\odot$–assuming a luminosity evolution proportional to the third power of the redshift–would be detected by SPIRE at a redshift greater than z $\simeq$ 4; by ASTRO-F at z $\simeq$ 1; by PACS at z $\simeq$ 3; by SIRTF at a redshift between 2 and an hypothetical z=10, from long to short wavelengths, respectively; by NGST

Table 1: Adopted SED, LLF and evolution for the different object classes

Object type	SED	LLF	evolution
QSO	Figure 2	Bo01	Bo01 + Bi01
Seyfert 1	Figure 1	Bo01	Bo01 + Bi01
Seyfert 1	Figure 1	RMS (Seyferts 1)	MS01
Seyfert 2	Figure 1	RMS (Seyferts 2)	MS01
Starburst	Figure 1	RMS (non-Seyfert)	MS01
Normal Galaxies	Figure 1	RMS (non-Seyfert)	MS01

Bo01: Boyle et al. (2001)

Bi01: Bianchi, Cristiani & Tae-Sum (2001)

RMS: Rush, Spinoglio & Malkan (1993)

MS01: Malkan & Stecker (2001)

Table 2: Expected counts of AGN and galaxies in future IR surveys in a $\Omega_\Lambda = 0$, $\Omega = 1$ Universe

λ (μm)	$S_{min}(5\sigma,1h)$ (μJy)	area (deg^2)	QSO	Sy 1 as QSO	Sy 1 as Sy 2	Sy 2	SB	gal	Instrument
4.5	13	0.3	5.0e2	3.0e3	4.5e3	3.0e3	5.7e4	2.0e4	IRAC/SIRTF
8.0	98	0.3	6.4e2	3.3e3	2.0e3	2.0e3	2.5e4	6.0e3	IRAC/SIRTF
24	550	0.3	1.8e3	2.0e3	9.0e2	1.0e3	1.3e4	4.0e3	MIPS/SIRTF
75	3000	1.0	4.0e3	3.6e3	1.1e3	1.1e3	6.0e3	1.3e3	PACS/Herschel
110	3000	1.0	...	3.0e3	1.3e3	1.6e3	1.2e4	3.6e3	PACS/Herschel
170	3000	1.0	...	6.0e3	2.8e3	2.7e3	1.3e4	5.5e3	PACS/Herschel

Table 3: Expected counts of AGN and galaxies in future IR surveys in a $\Omega_\Lambda = 0.7$, $\Omega_m = 0.3$ Universe

λ (μm)	$S_{min}(5\sigma,1h)$ (μJy)	area (deg^2)	QSO	Sy 1 as QSO	Sy 1 as Sy 2	Sy 2	SB	gal	Instrument
4.5	13	0.3	2.0e4	7.8e4	6.1e4	3.8e5	7.1e5	2.2e5	IRAC/SIRTF
8.0	98	0.3	2.6e4	4.8e4	3.4e4	1.6e4	2.2e5	1.2e5	IRAC/SIRTF
24	550	0.3	8.0e4	2.7e4	1.6e4	1.0e4	1.2e5	4.5e4	MIPS/SIRTF
75	3000	1.0	2.0e5	4.6e4	2.2e4	1.8e4	1.6e5	1.7e4	PACS/Herschel
110	3000	1.0	...	4.7e4	2.7e4	2.7e4	2.1e5	3.5e4	PACS/Herschel
170	3000	1.0	...	8.0e4	4.6e4	4.7e4	3.0e5	6.0e4	PACS/Herschel

at any redshift. The sensitivity of the all-sky survey that will be done with the Planck mission will not be sufficient to detect statistically significant numbers of galaxies beyond the Local Universe (unless these are gravitationally lensed). Because starburst galaxies have the steepest far-IR SED among the different classes and - especially - much steeper than the Seyfert 1's, at the same bolometric luminosity starburst galaxies can be more easily detected by far-IR/submillimeter space missions, while Seyfert 1's are favoured by near- and mid-IR instruments.

We should keep in mind that these $L_\star$ galaxies at z=4 will be swamped by hundreds of times more galaxies at lower redshifts. The median redshifts of the flux limited samples is 1.9, and around 3 percent of the total number of active and starburst galaxies will be at redshift larger than 3.

5. Confusion Limits

We now assess the implications of the above results for the confusion limits. Confusion arises because of the uncertain and varying contribution of flux density from the numerous unresolved faint sources that fall within each resolution element (or beam in diffraction-limited instruments). It depends on the details of both the shape of the counts and the clustering strength of the galaxies in the survey. Confusion becomes the dominant noise for any observations deeper than a certain limit, which generally corresponds to a density of sources in the sky that is greater than about 0.03/beam[2].

Confusion is a function of the beam size, θ_0, the source counts, $N(S)$, the cut-off related to the sources, $x_c = S_c \cdot \Psi(\theta, \phi)$, the response distribution, $R(x)$, and the q-parameter. The cutoff x_c is chosen usually to be q times $\sqrt{< \delta i >^2}$ where

$$(\delta i)^2 = \int_0^{x_c} x^2 R(x) dx \tag{3}$$

and $R(x) = \int \frac{dN(x/\Phi)}{dS} \frac{d\omega}{\Psi}$. The confusion function can then be written (see i.e. Franceschini et al., 1989; De Zotti et al., 1996; Väisänen et al., 2001):

$$\sigma_{conf} = f(\theta_0, N(S), x_c, S_c, q) \tag{4}$$

[2]the standard rule-of-thumb for which confusion becomes important is at 1/30 of a source per beam, a beam being one resolution element in the image

If differential counts follow a power-law behaviour, $\frac{dN(S)}{dS} \propto kS^{-(\delta+1)}$ then eq. 3 simplifies to $\sigma_{conf} = (\frac{q^{2-\delta}}{2-\delta})^{1/\delta}(k\Omega_e)^{1/\delta}$ where $\Omega_e = \int[\Psi(\theta,\phi)]^\delta d\omega]$ is the effective beam and Ψ the angular power pattern of the instrument.

In order to estimate the value of σ_{conf} at each wavelength, we sum up the contribution of each source population to the counts to integrate eq. 3. The resulting values are shown in table 4.

Although the adopted Universe models are quite extreme, and show a huge discrepancy in predicting source counts (see tables 2 and 3) the values reported in Table 4 can be considered as a reasonable range of possible limiting fluxes which should be considered when planning deep integrations.

The values are not in conflict with the sensitivities shown in tables 2 and 3. They represent very conservative limits due to source confusion which depends on the models we adopted. They mean, for instance, that IRAC at 4.5 μm will never be confusion limited for integration times shorter than 700 hours in a flat Universe with $\Omega_\Lambda = 0$, while after 2 hours its performance will be limited by source confusion in an open Universe with $\Omega_\Lambda > 0$. PACS at 75 μm will never be confusioned limited in both cases. At longer wavelengths the PACS instrument will always be confusion limited for integration time longer than 1 hour at 110 μm and 20 m at 170 μm, while MIPS at 24 μm reaches confusion limits in a $\Omega_\Lambda > 0$ Universe for integrations longer than nine hours.

Although the results of these computations are affected by uncertainties – linked to source evolution and Universe geometry –, they show that confusion will constitute a serious fundamental detection limit in these forthcoming experiments. Overcoming this limit will eventually require interferrometric observations, such as those anticipated at 350–450 μm by ALMA.

Table 4: Expected 5σ confusion limits for future instruments

λ (μm)	Ω_e (10^{-5} sr)	$\sigma_{conf}(\Omega_\Lambda = 0, \Omega = 1)$ (μJy)	$\sigma_{conf}(\Omega_\Lambda = 0.7, \Omega_{\rm mat} = 0.3)$ (μJy)	Instrument
4.5	.64	0.5	4	IRAC/SIRTF
8.0	1.2	3	30	IRAC/SIRTF
24	3.4	30	200	MIPS/SIRTF
75	2.4	30	600	PACS/Herschel
110	2.9	100	3000	PACS/Herschel
170	4.5	600	20000	PACS/Herschel

6. Colour-colour diagrams

Colour-colour diagrams of objects observed in multifrequency surveys are a powerful tool for identifying and classifying objects. In Figures 7 and 8 the colour-colour diagrams [4.5 - 8] versus [8 - 24] and [8 - 24] versus [24-70] [3] are presented. In these two diagrams redshift tracks, computed from redshifts of 0 to 4, are shown for each type of galaxy. These tracks identify the locus on the diagram where object colours are expected to lie, and can be then exploited to pinpoint candidates for follow-up observations.

To avoid confusion with galactic stellar objects, we also plot in Figure 7 the average colours of Class I protostars (Nielbock et al. 2001), while Class 0 protostars (Andre et al. 2000), and brown dwarfs (Martín et al. 2001) are, respectively, too red and too blue in at least one colour to fall within the limits of this diagram. The diagrams in Figures 8 are never affected by the presence of stellar objects.

In the [4.5 - 8] vs [8 - 24] diagram (Figure 7) a clear separation occurs among the three classes of galaxies: quasars, Seyfert 1's and starburst galaxies. Their tracks are constrained by: $0.6 < [8-24] < 0.9$ and $[4.5-8] > 0.8$, $[8-24] > 1.0$ and $[4.5-8] > 0.9$, $0.5 < [8-24] < 0.9$ and $[4.5-8] < 0.5$, respectively. However, both Seyfert 2's and normal galaxies lie in a region which is intermediate between Seyfert 1's and starburst galaxies. Therefore it would not be possible to distinguish them solely on the basis of 4.5-8-24μm photometry.

The [8 - 24] vs [24 - 70] diagram (Figure 8) shows that quasars and Seyfert 1's are both well segregated from starbursts, Seyfert 2's and normal galaxies, and can be selected by [8 - 24]>0.9 and [24 - 70]>0.8. However, these three latter galaxy classes do overlap each other in these colours. Starbursts and Seyfert 2's are almost indistinguishable in this diagram, and normal galaxies share most of their colours except at small redshifts where [24 - 70]>0.7.

In the diagrams in Figures 7 and 8 the average local SED of each type of galaxies is considered, assuming no scatter. To have a better estimate of the power of the two colour-colour diagrams in separating different classes of objects and of their limits, we have estimated the likely errors in the colours and included them in the figures, assuming that the flux densities in the three bands have uncertainties of 20%.

These colour-colour plots are affected by a redshift degeneracy: higher-redshift Seyfert 2's resemble the lower-redshift starburst galaxies. For most objects the redshift will not be known. Using more than just 3 filters simultaneously will help in sorting this out. In fact, some tracks are smooth enough that it is possible to fit a simple analytic formula for each

[3] we use as colour definition: $[\lambda_1 - \lambda_2] = d \log \frac{(F_1/F_2)}{\lambda_1/\lambda_2}$, where F_i are flux densities.

type of galaxy:

$$z_{\text{object type}} = A[4-8] + B[8-24] + C[24-70] + D[4-8]^2 + E[8-24]^2 + F[24-70]^2 \quad (5)$$

with coefficients given in Table 5.

Evolution from one class of galaxies to another has not been considered, as well as other speculative assumptions, because we want to keep this work as much as possible on a firm empirical basis.

7. Conclusions

- In this paper we predict, on an empirical basis, active and normal galaxy counts which future space missions will be able to measure in the far-IR. The observed SEDs of different types of objects (Seyfert 1 and 2, starburt, normal galaxies and QSOs) are evolved backwards in time, using our present knowledge of their local luminosity functions and their evolution.

- The number of Seyfert 1 and 2, Starbursts and normal galaxies that should be detected in future surveys are shown in Tables 2 and 3 and Figures 4 and 5. In the most conservative case (a flat Universe $\Omega_\Lambda = 0$, $\Omega = 1$), SIRTF and Herschel will be able to detect from thousands to tens of thousands of active and starburst galaxies in a field of 0.3 and 1 deg^2, respectively. Our results are affected by the following uncertainties:

  - Type 1 QSOs: their evolution has a solid foundation since the B-band LF is well known at least up to redshift 3. Their far-IR SED is however very uncertain. We use the composite spectrum shown in Figure 2 whose photometric uncertainty is large (see Andreani et al., 2003 for details).

Table 5: Fitting coefficients for photometric redshift estimates

Object type	A	B	C	D	E	F
starburst	.096	1.88	.05	.73	.41	.84
Seyfert 1's	.310	1.85	3.03	-.69	-.95	.22
Seyfert 2's	.990	1.95	0.31	-.13	.26	.85
normal galaxies	.460	1.42	0.74	-.56	.43	.64
Quasars	-.160	1.99	-0.05	-1.14	.40	.34

  - Nearby Seyfert and Starburst galaxies on the contrary have a well-defined average SED, but the knowledge of their evolution is poor. Future far-IR Space missions, mainly SIRTF, will eliminate this uncertainties.

- Colour-colour diagrams are constructed from the SEDs shown in Figures 2 and 1, without evolution taken into account. Curves are very uncertain for QSOs, because of their poorly determined far-IR SED. Colour-colour diagrams with the selected frequency bands will be a powerful tool for discriminating among different object types: quasars from Seyfert 1's, Seyfert 2's and starburst galaxies. Redshift measurements (or estimates) can be used to resolve the degeneracy present in some cases.

- The confusion-limiting flux tends to be high compared with the limiting sensitivity of both SIRTF and Herschel instruments. Instrument teams are indeed seriously considering it for very long exposures.

- SIRTF will make fundamental discoveries about AGN evolution, exploiting mainly the 8 and 24 μm bands. These bands are critical to selecting unbiased samples of type 1 and 2 AGN.

PA acknowledges the Infrared Group of the Max-Planck Institut für Extraterrestrische Physik of Garching (Germany) for hospitality during the first stage of this work. The Italian Space Agency (ASI) has funded part of this work under the contract ASI-I-R-037-01.

REFERENCES

André P., Ward-Thompson D., Barsony M., 2000 Protostars & Planets IV, eds. V. Mannings, A. Boss, S. Russell (Tucson: The Univ ersity of Arizona Press), 59.

Andreani P. et al., 2003, AJ 125, 444

Bianchi S., Cristiani S., Tae-Sum K., 2001, A&A 376, 1

Boyle B.J. et al., 2001, MNRAS 317, 1014

Chapman S.C., Smail I., Ivison R.J., Helou G., Dale D.A., and Lagache G., 2002, ApJ 573, 66

De Zotti G., Franceschini A., Toffolatti A., Mazzei P., Danese L., 1996, Astr. Lett. Com. 35, 289

Fang F., Shupe D.L., Xu C., Hacking P.B., ApJ 500, 693 (San Francisco)

Franceschini A., Toffolatti A., Danese L., De Zotti G., 1989, ApJ 344, 35

Franceschini, A. 2000, in "Galaxies at High Redshift", F.Sanchez, I.Perez-Fournon, M.Barcells, F.Moreno-Insertis Eds., Cambridge University Press, in press (astro-ph/0009121)

Granato G.L., Danese L., 1994, MNRAS 268, 235

Granato et al., 2001, MNRAS 324, 757

Hooper E.J. et al., 1999, in Proc. of "The Universe as seen by ISO", ed. M.Kessler, ESA-SP 427

Lagache G., Dole H., Puget J.L., MNRAS in press, astro-ph/0209115

La Franca F., & Cristiani S., 1998, AJ113, 1517, and AJ 115, 1688

Malkan M.A. & Stecker F.W. 1998, ApJ 496, 13

Malkan M.A. & Stecker F.W. 2001, ApJ 555, 641

Martín E.L., Brandner W., Jewitt D.C., Simon T., Wainscoat R., Connelley M, 2001, PASP 113, 529

Nielbock M., Chini R., Jütte M., Manthey E., 2001, A&A 377,273

Polletta M., Courvoisier T.J.-L., Hooper E.J., Wilkes B.J., 2000, A&A 362, 75

Rush B., Malkan M.A. & Spinoglio L., 1993, ApJS 89,1 (RMS)

Silk J. and Rees M., 1998, A&A 331, L1

Spinoglio L. and Malkan, M.A. 1989, ApJ '342, 83

Spinoglio L. et al. 1995, ApJ 453,616

Spinoglio L., Andreani P. & Malkan, M.A. 2002, ApJ 572, 105

Thean A. et al 2001, MNRAS325, 737

Tran H.D. 2001, ApJ554, L19

Väisänen P., Tollestrup E.V., Fazio G.G, 2001, MNRAS

Wilkes B.J. et al.., 1999, in Proc. of "The Universe as seen by ISO", ed. M.Kessler, ESA-SP 427

Xu C., Hacking P., Fang F. et al. 1998, ApJ 508, 576

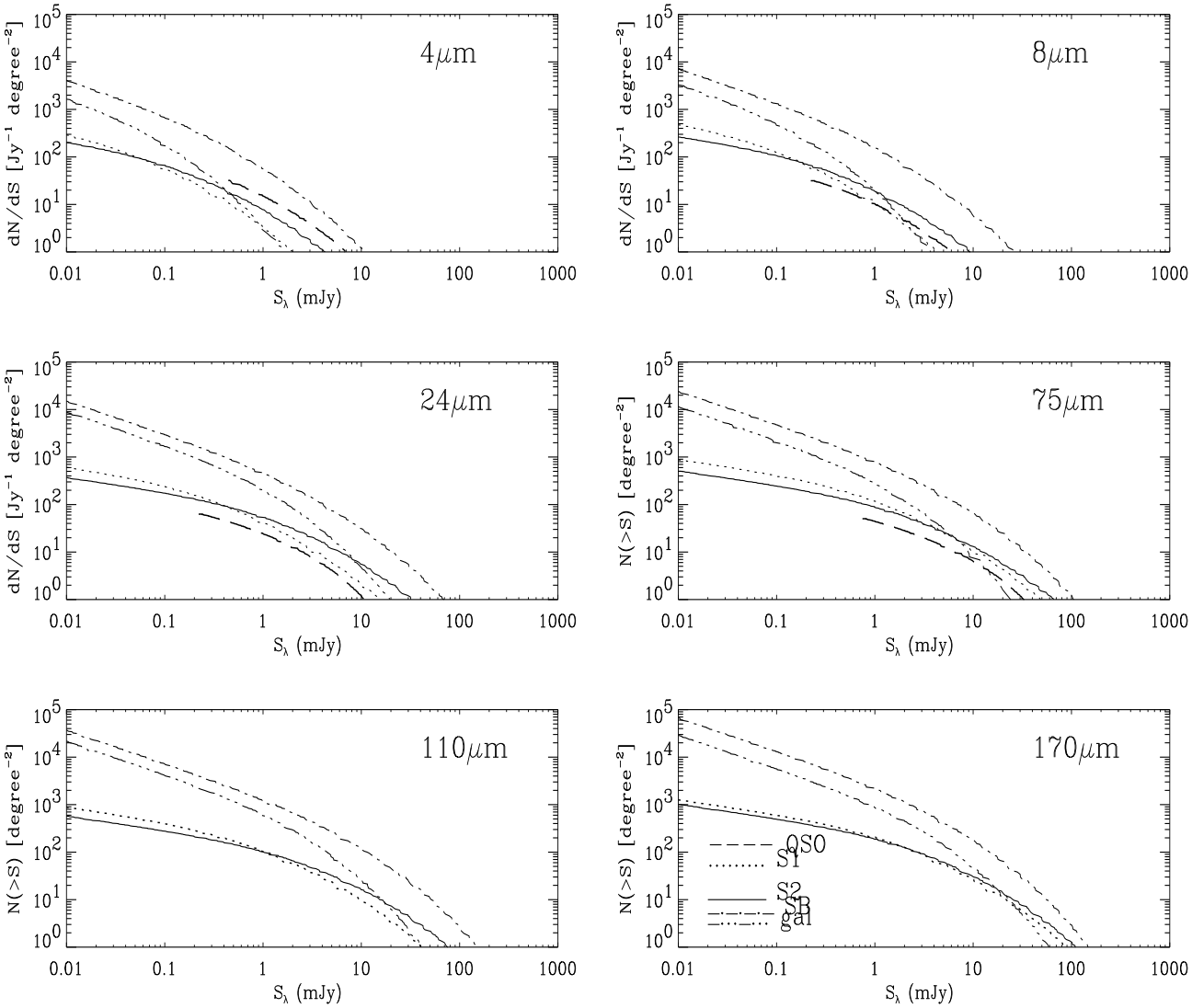

Fig. 4.— Expected differential number counts of type 1 QSO, Seyfert, starburst and normal galaxies computed from the composite SEDs presented in this work, for a Universe with Ω_Λ=0, $\Omega_{\rm mat}$ = 1. The different wavelengths correspond to the bands of IRAC (4.5 and 8 μm) and MIPS (24μm) instruments on board SIRTF and PACS (75, 110 and 170μm) on board Herschel.

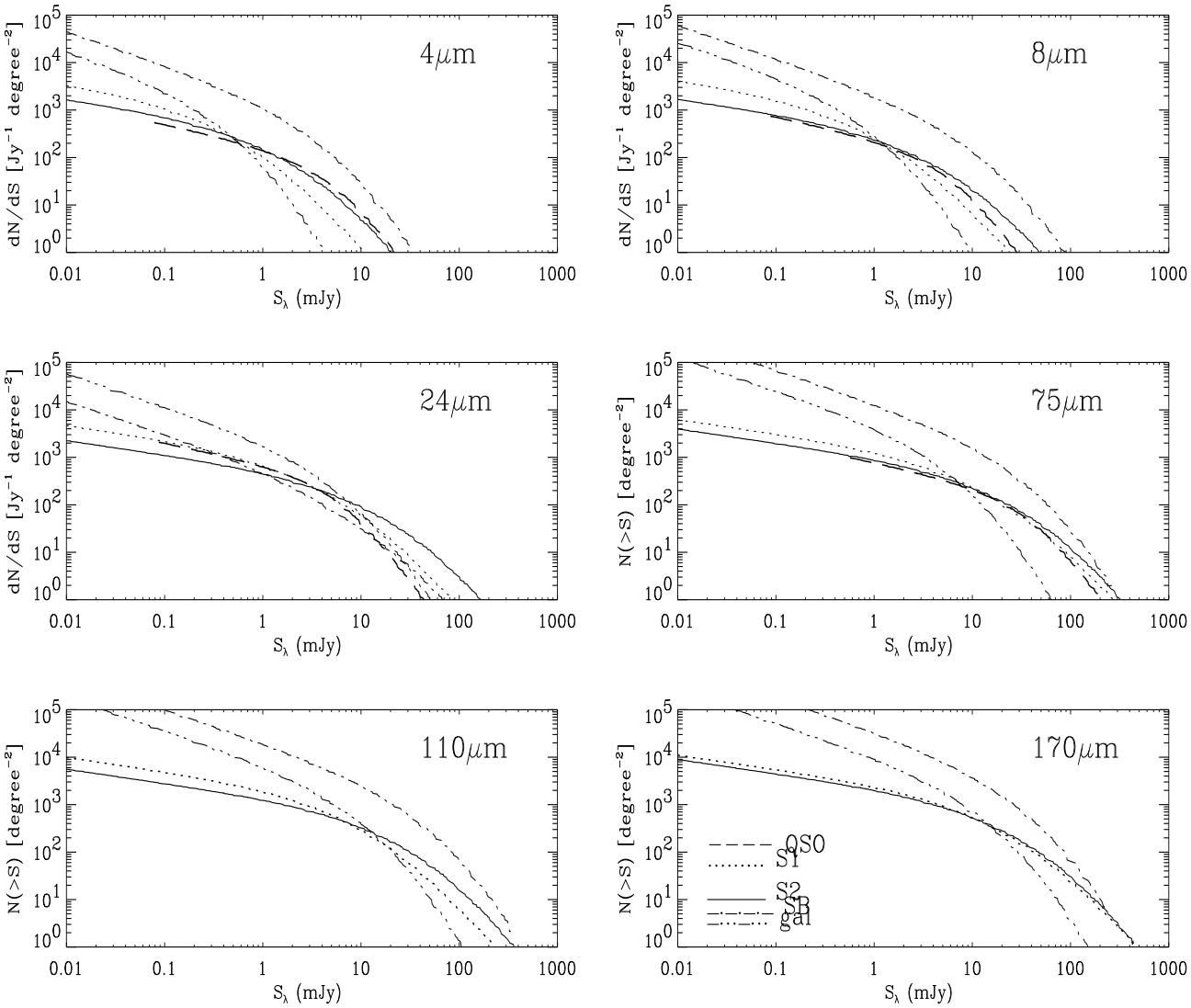

Fig. 5.— Same as Figure 4 but for a Universe with $\Omega_\Lambda = 0.7$, $\Omega_{\rm mat} = 0.3$

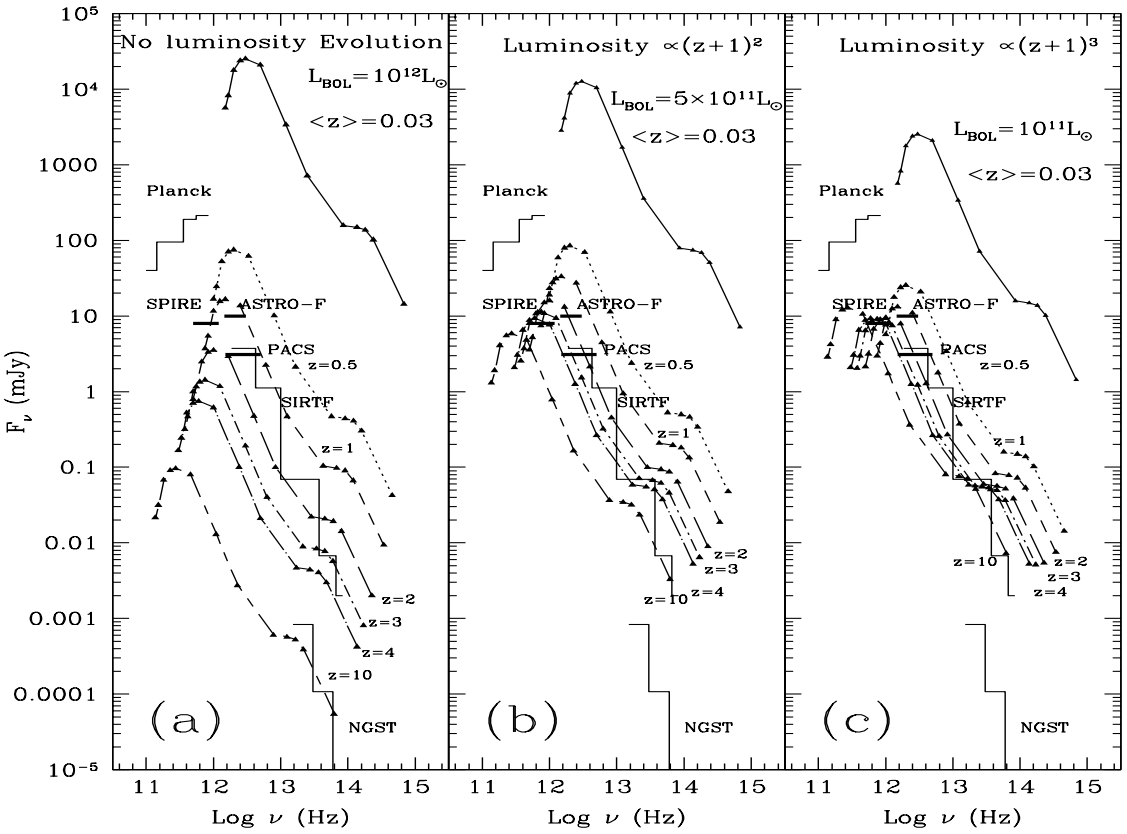

Fig. 6.— Predicted SEDs of starburst galaxies as a function of redshift, compared to the expected sensitivities (5σ, 1 hr.) of the future space missions Herschel, Planck, SIRTF, ASTRO-F and NGST with 3 different model assumptions. (a): SED of a galaxy with $L_{BOL} = 10^{12}L_\odot$, assuming no luminosity evolution; (b): SED of a galaxy with $L_{BOL} = 5\times10^{11}L_\odot$, assuming $(z+1)^2$ luminosity evolution; (c): SED of a galaxy with $L_{BOL} = 10^{11}L_\odot$, assuming $(z+1)^3$ luminosity evolution.

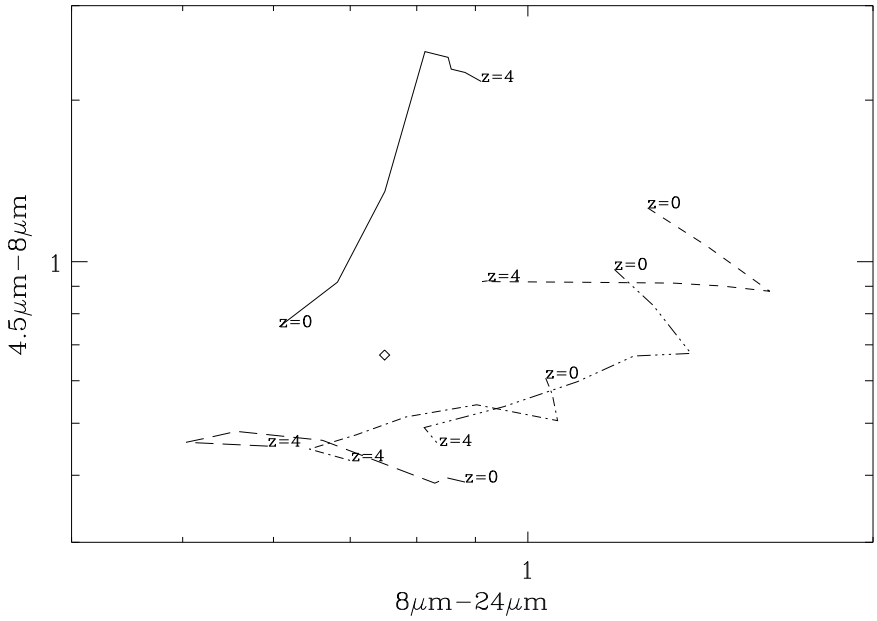

Fig. 7.— Redshift tracks for QSO (solid line), Seyfert 1 (dash), Seyfert 2 (dash-dot), starburst (long dash) normal (dash dot dot dot) galaxies from z=0 to z=4. The diamond refers to the most extreme measured values of these colours for class I protostars (Nielbock et al. 2001).

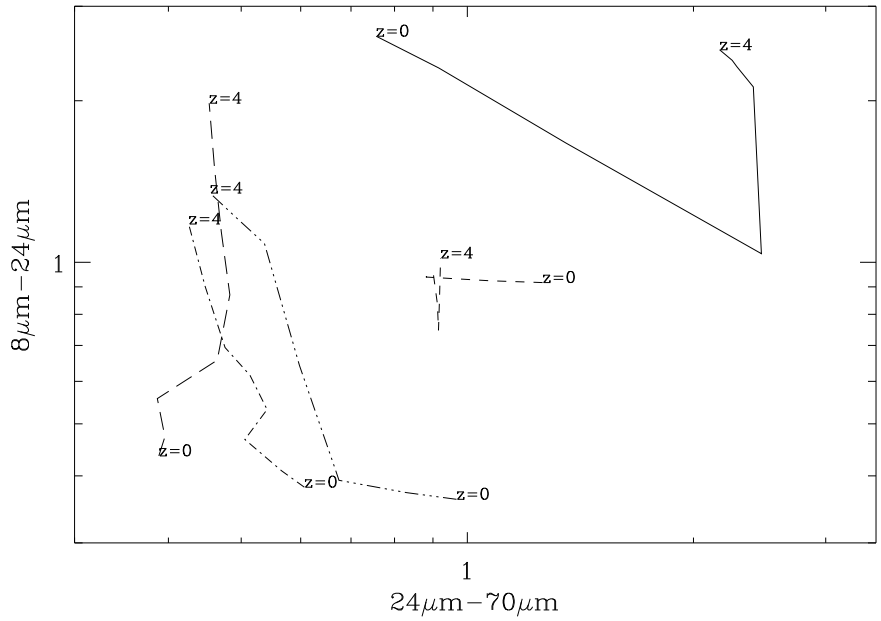

Fig. 8.— Redshift tracks for QSO (solid line), Seyfert 1 (dash), Seyfert 2 (dash-dot), starburst (long dash) normal (dash dot dot dot) galaxies from z=0 to z=4.